



**HAL**  
open science

## High-Temperature Thermoelectric Properties of Sn-Doped $\beta$ -As<sub>2</sub>Te<sub>3</sub>

Jean-Baptiste Vaney, Julie Carreaud, Gaëlle Delaizir, Annie Pradel, Andrea Piarristeguy, Cédric Morin, Eric Alleno, Judith Monnier, Pereira Antonio, Christophe Candolfi, et al.

► **To cite this version:**

Jean-Baptiste Vaney, Julie Carreaud, Gaëlle Delaizir, Annie Pradel, Andrea Piarristeguy, et al.. High-Temperature Thermoelectric Properties of Sn-Doped  $\beta$ -As<sub>2</sub>Te<sub>3</sub>. *Advanced Electronic Materials*, 2015, 1 (1-2), pp.1400008. 10.1002/aelm.201400008 . hal-01111957

**HAL Id: hal-01111957**

**<https://hal.science/hal-01111957>**

Submitted on 23 Feb 2023

**HAL** is a multi-disciplinary open access archive for the deposit and dissemination of scientific research documents, whether they are published or not. The documents may come from teaching and research institutions in France or abroad, or from public or private research centers.

L'archive ouverte pluridisciplinaire **HAL**, est destinée au dépôt et à la diffusion de documents scientifiques de niveau recherche, publiés ou non, émanant des établissements d'enseignement et de recherche français ou étrangers, des laboratoires publics ou privés.

# High-Temperature Thermoelectric Properties of Sn-Doped $\beta$ -As<sub>2</sub>Te<sub>3</sub>

Jean-Baptiste Vaney, Julie Carreaud, Gaëlle Delaizir, Annie Pradel, Andrea Piarristeguy, Cédric Morin, Eric Alleno, Judith Monnier, Antonio Pereira Gonçalves, Christophe Candolfi, Anne Dauscher, and Bertrand Lenoir\*

Thermoelectric energy conversion is a versatile and an all-solid-state technology that can be used either in cooling systems (Peltier effect) or in electrical power generators (Seebeck effect). Because thermoelectric generators convert directly temperature differences into electrical power, this technology, thanks to its reliability, long lifetime, and vibration-free character, has been successfully used for decades for powering deep space missions. Thermoelectric generators may be equally suitable for waste-heat recovery from automotive exhaust systems or various industrial processes. Near room temperature, Peltier coolers are applied as solid-state heat pumps for cooling electronic devices, for instance.<sup>[1,2]</sup>

The active parts of thermoelectric devices are composed of *n*- and *p*-type materials whose intrinsic transport properties govern the overall conversion efficiency. The potential of a given material for thermoelectric applications is quantitatively expressed by the dimensionless figure of merit *ZT* defined as  $ZT = \alpha^2 T / \rho(\kappa_e + \kappa_l) = PT / (\kappa_e + \kappa_l)$  where  $\alpha$  is the thermopower (or Seebeck coefficient),  $\rho$  is the electrical resistivity,  $\kappa_e$  and  $\kappa_l$  are the electronic and lattice thermal conductivities, respectively, *T* is the absolute temperature, and  $P = \alpha^2 / \rho$  is the power factor. Achieving high *ZT* on a broad temperature range represents the most critical and challenging aspect in thermoelectricity.<sup>[3,4]</sup>

The binaries (Bi,Sb)<sub>2</sub>X<sub>3</sub> (*X* = Se, Te) stand for end-members of the quaternary (Bi,Sb)<sub>2</sub>(Se,Te)<sub>3</sub> thermoelectric alloys which remain to date the most efficient thermoelectric materials for room-temperature applications.<sup>[1,2]</sup> When both *n*-type and *p*-type compounds are optimized, *ZT* values around unity are achieved near 300 K. Over the last years, these well-known thermoelectric materials were revisited, leading to their classification as three-dimensional topological insulators.<sup>[5–13]</sup> This distinct state of matter is characterized by bulk electronic band gap and gapless electronic surface states displaying linear, photon-like energy dispersions. In contrast to thermoelectric materials that should possess low electrical resistivity, highly resistive samples are intensively sought in this area of research in order to facilitate the observation of signatures of the surface states in the transport properties.<sup>[14–20]</sup>

$\beta$ -As<sub>2</sub>Te<sub>3</sub> is one of the two allotropic forms of As<sub>2</sub>Te<sub>3</sub> (together with  $\alpha$ -As<sub>2</sub>Te<sub>3</sub>) and represents another member of this family of compounds crystallizing in the rhombohedral  $R\bar{3}m$  space group.<sup>[21,22]</sup> It is thus no surprise that this material was recently proposed to also harbor topological surface states.<sup>[23]</sup> Yet, because the strength of the spin-orbit coupling is lower in  $\beta$ -As<sub>2</sub>Te<sub>3</sub> than in Bi<sub>2</sub>Te<sub>3</sub> due to the lighter mass of As—an essential requirement in obtaining a topological state—the transition from a trivial band insulator to a topological insulator necessitates high pressures (1.8 GPa).<sup>[23]</sup> From calculations of its electronic band structure and phonon dispersions, it was concluded that  $\beta$ -As<sub>2</sub>Te<sub>3</sub> might as well show interesting thermoelectric properties, akin to those observed in the Bi-based counterparts. An indirect band gap of  $\approx 0.2$  eV in the *Z*-*F* direction of the Brillouin zone and acoustic phonon frequencies limited to 50 cm<sup>-1</sup> are the two main characteristics that were suggested to lead to high power factors and low thermal conductivity, respectively, and hence, high *ZT* values.<sup>[23]</sup> These calculations, that take into account the spin-orbit coupling, are in agreement with prior theoretical and experimental studies yielding 0.22 and 0.13 eV, respectively.<sup>[21,24]</sup>

Early studies have reported  $\beta$ -As<sub>2</sub>Te<sub>3</sub> as a high-pressure phase obtained from a pressure-induced structural transition of the monoclinic derivative  $\alpha$ -As<sub>2</sub>Te<sub>3</sub> near 7 GPa.<sup>[21]</sup> Further experimental work has suggested that quenching procedures are sufficient to directly synthesize bulk samples of  $\beta$ -As<sub>2</sub>Te<sub>3</sub>.<sup>[22]</sup> Yet, unlike the Bi-based alloys and despite the possibility to synthesize samples under ambient pressure, the transport properties of  $\beta$ -As<sub>2</sub>Te<sub>3</sub> remain so far largely unexplored.

Herein, we report on the successful synthesis of phase-pure samples of  $\beta$ -As<sub>2</sub>Te<sub>3</sub> and show that the carrier concentration can be tuned by substituting Sn for As. A maximum *ZT* value

Dr. J.-B. Vaney, Dr. C. Candolfi, Dr. A. Dauscher,  
Prof. B. Lenoir  
Institut Jean Lamour  
UMR 7198 CNRS – Université de Lorraine  
Parc de Saurupt, CS 50840  
54011 Nancy, France  
E-mail: bertrand.lenoir@univ-lorraine.fr



Dr. J. Carreaud, Dr. G. Delaizir  
Sciences des Procédés Céramiques et de Traitement de Surface (SPCTS)  
UMR CNRS 7315, Centre Européen de la Céramique  
12 rue Atlantis, 87068 Limoges, France

Dr. J.-B. Vaney, Dr. A. Pradel, Dr. A. Piarristeguy  
Institut Charles Gerhardt Montpellier (ICGM)  
UMR 5253 CNRS-Université Montpellier, 2 Place Eugène Bataillon,  
34000 Montpellier, France

Dr. C. Morin, Dr. E. Alleno, Dr. J. Monnier  
Institut de Chimie et des Matériaux Paris Est (ICMPE)  
UMR 7182 CNRS, Université Paris-Est Créteil  
2-8 rue Henri Dunant, 94320 Thiais, France

Dr. A. P. Gonçalves  
C2TN, Instituto Superior Técnico  
Universidade de Lisboa  
P-2686-953 Sacavém, Portugal

DOI: 10.1002/aelm.201400008

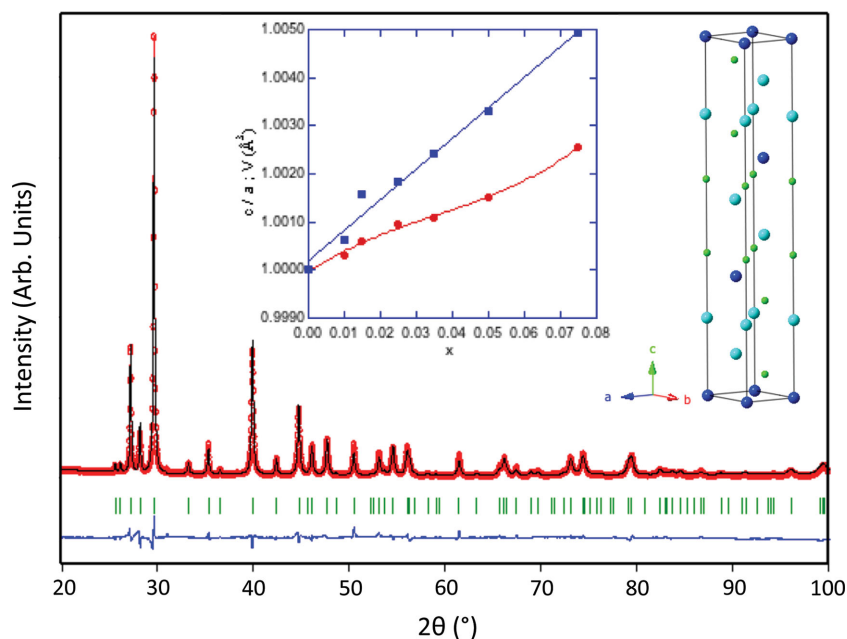


**Figure 1.** Powder X-ray diffraction pattern of  $\beta\text{-As}_2\text{Te}_3$ . The observed data are marked as open red circles. The calculated profile is represented by a solid black line while the difference between experimental and calculated patterns is shown by a lower solid blue line ( $R_f = 7.41$ ,  $\chi^2 = 2.23$ ). The positions of the Bragg reflections are indicated as green bars. The right inset illustrates a perspective view of the crystal structure of  $\beta\text{-As}_2\text{Te}_3$  (the As atoms are represented by small green balls and the Te atoms by large dark and sky blue balls). The middle inset shows the  $c/a$  ratio (●) and the unit cell volume  $V$  (■) of  $\beta\text{-As}_{2-x}\text{Sn}_x\text{Te}_3$  as a function of the Sn content. All the values of  $c/a$  and  $V$  were normalized to the respective room-temperature ratio. The solid blue line is the best linear fit to the data while the solid red curve is a guide to the eye.

of 0.65 is achieved at 423 K thanks to a beneficial combination of high power factor and extremely low thermal conductivity values. Our results evidence that high thermoelectric efficiency may be achieved in  $\beta\text{-As}_2\text{Te}_3$  through a proper optimization of the carrier concentration by substitutions. In addition, the fact that this allotropic form can be easily synthesized under ambient pressure may pave the way toward the growth of single crystals of undoped and doped  $\beta\text{-As}_2\text{Te}_3$ , an essential prerequisite to investigating its possible topological surface states.

**Figure 1** shows the powder X-ray diffraction (PXRD) pattern of  $\beta\text{-As}_2\text{Te}_3$ . All reflections can be indexed in the  $R\bar{3}m$  space group with no evident sign of impurities. Similar conclusions can be drawn from the PXRD patterns collected for the Sn-doped samples except for  $x = 0.015$  where a small additional peak ascribed to the AsTe phase ( $Fm\bar{3}m$ ,  $a = 5.778 \text{ \AA}$ ) is observed (Figure S1, Supporting Information).

These data are thus consistent with both the successful synthesis of pure  $\beta\text{-As}_2\text{Te}_3$  and the effective insertion of Sn into the crystal structure. Due to the significant anisotropy in the crystal structure, the samples show a preferred orientation resulting in a slight renormalization of the relative intensities of the Bragg reflections. Nonetheless, the Rietveld refinements of the diffraction patterns lead to good fits to the data, which allow for a precise determination of the lattice parameters. The lattice parameters of the  $x = 0$  sample ( $a = 4.0473 \text{ \AA}$  and  $c = 29.5018 \text{ \AA}$ ) are in agreement with literature data.<sup>[22,25]</sup> With increasing the Sn content up to  $x = 0.075$ , the unit cell

volume expands quasi linearly reflecting the monotonic increase along the  $a$  and  $c$  axes, the latter increasing with a steeper slope with respect to the former. The slight but noticeable change of slope near  $x = 0.030$  (see inset of Figure 1) might be due to deviations of the actual Sn content from the nominal compositions, higher  $x$  values resulting in larger deviations. However, if proven to be intrinsic, this change in behavior might hint at structural differences in the crystal structures below and above this concentration. In  $\text{Bi}_2\text{Te}_3$  or  $\text{Bi}_2\text{Se}_3$ , it is well-known that extrinsic dopants such as Cu may either intercalate between the Te or Se layers or randomly substitute for Bi.<sup>[26–28]</sup> Alternatively, Sn might behave as an amphoteric dopant in  $\beta\text{-As}_2\text{Te}_3$ , i.e., Sn might substitute simultaneously for As and Te, as observed for some specific elements in  $\text{PbTe}$  or  $\text{Sb}_2\text{Te}_3$  thermoelectric alloys.<sup>[29–31]</sup> Scanning electron microscopy (SEM) and X-ray mapping further revealed an overall homogeneous distribution of the different elements in the samples regardless of the composition (Figures S2,S3, Supporting Information).

The temperature dependences of  $\alpha$  and  $\rho$  measured parallel and perpendicular to the pressing directions are shown in **Figures 2a,b**, respectively. In undoped  $\beta\text{-As}_2\text{Te}_3$ , the values of  $\alpha$  are positive indicating that holes are the dominating charge carrier type. Upon heating, the magnitude of  $\alpha$  increases linearly from  $\approx 110 \mu\text{V K}^{-1}$  at 300 K up to  $155 \mu\text{V K}^{-1}$  at 423 K. Of note, the room-temperature value ( $\approx 110 \mu\text{V K}^{-1}$ ) is lower than those calculated from the Boltzmann transport equations ( $223 \mu\text{V K}^{-1}$ ) by Sharma and Srivastava<sup>[24]</sup> and measured by Scheidemantel et al.<sup>[21]</sup> ( $225 \mu\text{V K}^{-1}$ ). This difference suggests that the present sample is intrinsically heavily doped by acceptors and may be considered as an experimental evidence that intrinsic native defects and deviations from stoichiometry are also important factors in determining the carrier concentration in  $\beta\text{-As}_2\text{Te}_3$  as in  $\text{Bi}_2\text{Te}_3$ -based compounds.<sup>[1,2]</sup> Even though the difference between the values measured in the two directions lies at the border of the experimental uncertainty, the data exhibit a slight anisotropy that seems to decrease with increasing temperature.

The substitution of Sn for As has several important implications on the  $\alpha(T)$  data. A significant increase in  $\alpha$  with increasing  $x$  occurs up to  $x = 0.025$  where a maximum value of  $180 \mu\text{V K}^{-1}$  at 423 K is achieved. Above this concentration, this trend reverses, i.e., a decrease with  $x$  is observed which remains unaffected by further increasing  $x$  to  $x = 0.075$ . In addition, the anisotropy is no longer visible, the measurements in both directions being similar to within experimental accuracy. None of the samples enter the intrinsic regime of conduction that would be reflected by a maximum in  $\alpha(T)$  at high temperatures.

The overall variations in the  $\rho(T)$  data with  $x$  are consistent with the trend observed in  $\alpha(T)$  (Figure 2b). The metallic-like dependence of the  $x = 0$  sample progressively turns into

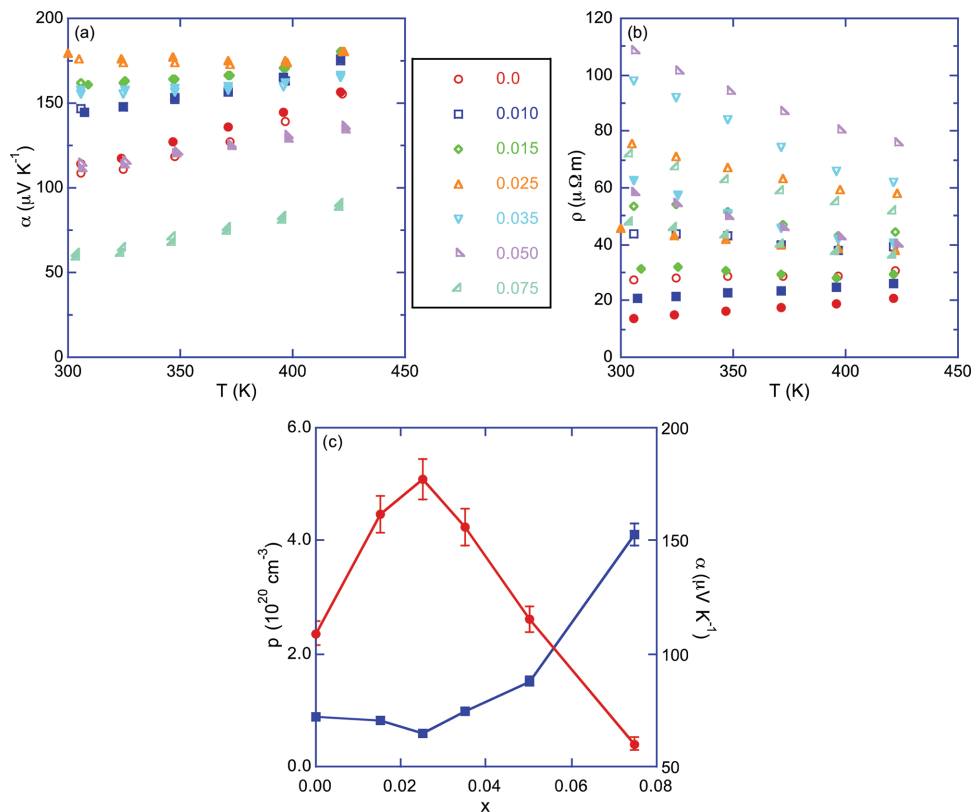


**Figure 2.** Temperature dependence of the thermopower  $\alpha$  a) and the electrical resistivity  $\rho$  b) of the polycrystalline  $\beta\text{-As}_{2-x}\text{Sn}_x\text{Te}_3$  samples. The measurements performed parallel and perpendicular to the pressing direction are represented by open and filled symbols, respectively. The composition color-coded is identical in both panels. c) Compositional dependence of  $\alpha$  (red circles) and  $\rho$  (blue squares) measured in the parallel direction at 300 K. The lines are guides to the eye.

a semiconducting behavior with increasing  $x$ . The  $\rho$  values measured perpendicularly to the pressing direction are systematically lower than those measured in the parallel direction, a property shared by the Bi- and Sb-based analogues. In contrast to  $\alpha$ , the anisotropy of the  $x = 0$  sample is also clearly observable in the Sn-doped samples and tends to decrease with increasing temperature, especially at the lowest substitution levels. At 300 K, the anisotropic character of the transport displays a nonmonotonic variation with the Sn content (Figure S4, Supporting Information). This property suggests that the anisotropy depends on the carrier concentration, likewise  $\text{Bi}_2\text{Te}_3$ -based alloys, which features a complex dependence of the anisotropy with the electron or hole concentration.<sup>[1,2]</sup>

The Hall carrier concentration  $n_{\text{H}}$  and Hall mobility  $\mu_{\text{H}}$  were evaluated at room temperature from measurements of the Hall coefficient  $R_{\text{H}}$ . All samples show positive  $R_{\text{H}}$  values suggestive of a dominant hole-like signal, in agreement with  $\alpha(T)$ . The hole density  $p$  first decreases from  $8.9 \times 10^{19}\text{ cm}^{-3}$  in the  $x = 0$  sample down to  $5.8 \times 10^{19}\text{ cm}^{-3}$  for  $x = 0.025$  before increasing to  $4.1 \times 10^{20}\text{ cm}^{-3}$  for  $x = 0.075$ . While these values are comparable to those typically observed in  $\text{Bi}_2\text{Te}_3$  alloys,<sup>[1,2]</sup> the measured value in the undoped sample is significantly higher than that predicted from first-principles calculations ( $1.19 \times 10^{19}\text{ cm}^{-3}$ ) in agreement with the lower  $\alpha$  values.<sup>[24]</sup> The values of the Hall mobility  $\mu_{\text{H}}$  are low, of the order of few tenths of  $\text{cm}^2\text{ V}^{-1}\text{ s}^{-1}$ , in

agreement with the hole concentration measured and the polycrystalline nature of the samples. The  $\mu_{\text{H}}(T)$  data follows a  $T^{-3/2}$  law indicating that acoustic phonon scattering dominates the hole scattering mechanisms in this temperature range.

In a simple picture, Sn atoms are expected to provide additional holes thereby driving the system toward a degenerate behavior. However, the compositional dependence of the electrical properties shown in Figure 2c reveals that  $\alpha$  does not monotonically vary with  $x$  but first increases, then shows a maximum near  $x = 0.025$  before decreasing at higher doping levels. Because the  $x = 0$  sample appears as intrinsically heavily doped, the behavior at low Sn contents may be related to a decreased amount of electrically active defects present in the sample upon doping with Sn. It is well established that the dominant native defects in  $\text{Bi}_2\text{Te}_3$ – $\text{Sb}_2\text{Te}_3$  mixed crystals are antisite defects  $\text{Sb}_{\text{Te}}$  or  $\text{Te}_{\text{Sb}}$ ,<sup>[1,2,32]</sup> whose formation is strongly influenced by the bond polarity.<sup>[32]</sup> Low bond polarity favors antisite defects since their energy formation is low. Because a weak difference in electronegativity between atoms decreases the bond polarity, the concentration of antisite defects can increase depending on the nature of the dopant. Since the Pauling electronegativity (PE) of As (PE = 2.18) and Te (PE = 2.10) are nearly equivalent (this difference is similar as that between Bi (PE = 2.02) and Sb (2.05) or Te (PE = 2.10)), antisite defects are also likely the prominent defects in  $\beta\text{-As}_2\text{Te}_3$ . Within this scenario, doping with an element that exhibits a larger or smaller electronegativity than

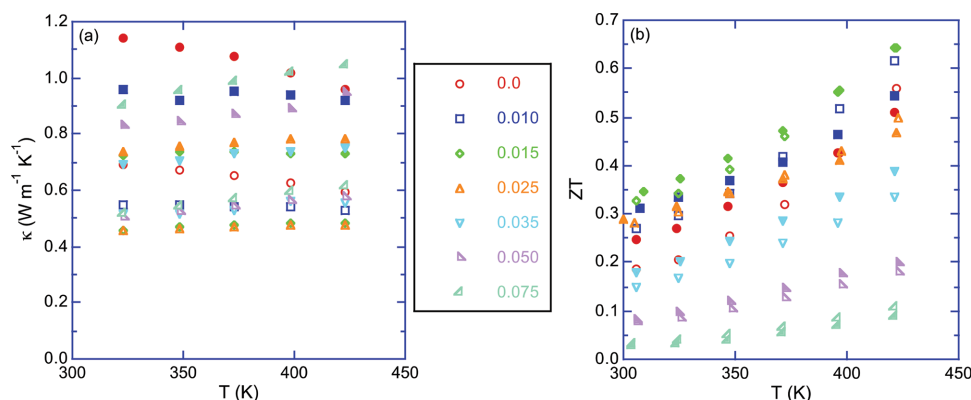


**Figure 3.** Temperature dependence of the total thermal conductivity  $\kappa$  (a) and the dimensionless figure of merit  $ZT$  (b) of the polycrystalline  $\beta$ - $\text{As}_{2-x}\text{Sn}_x\text{Te}_3$  samples. The measurements performed parallel and perpendicular to the pressing direction are represented by open and filled symbols, respectively. The composition color-coded is identical in both panels.

As can increase the bond polarity and hence, suppress antisite defects. As a consequence, a change in the carrier concentration is expected. Several dopants such as In (PE = 1.78) or Ga (PE = 1.81)<sup>[33,34]</sup> have been shown to effectively suppress the antisite defects in  $\text{Sb}_2\text{Te}_3$  and despite the fact that In and Ga belong to the group III elements, both act as donors. The case of Sn (PE = 1.96) in  $\text{Sb}_2\text{Te}_3$  is more complex since its amphoteric character was reported by Santhanam et al.,<sup>[35]</sup> even though Kulbachinskii et al.<sup>[36]</sup> have only reported an acceptor character in single crystals. At low Sn contents (below 2 at.%), Sn acts as a donor while at doping levels higher than 3 at.% Sn acts as an acceptor. Our findings, reminiscent to this behavior, suggest that Sn may behave similarly in  $\beta$ - $\text{As}_2\text{Te}_3$  and thus, may not act as a simple acceptor.

Figure 3a shows the temperature dependence of the total thermal conductivity. The temperature dependence of the specific heat used to calculate  $\kappa$  is shown in Figure S5 (Supporting Information). In the undoped sample,  $\kappa$  monotonically decreases with increasing temperature in a nearly equivalent manner in the parallel and perpendicular directions. The  $\kappa(T)$  data roughly follow a  $T^{-1}$  law suggesting that Umklapp scattering events dominate the thermal transport in this temperature range. The anisotropic behavior is akin to that unveiled by the  $\rho(T)$  data, even though an opposite trend is observed, the perpendicular direction exhibiting higher values compared to the parallel direction. Owing to the relatively high  $\rho$  values displayed by the Sn-doped compounds, the electronic contribution only weakly contributes to the thermal transport. The  $\kappa$  values measured in the parallel direction are extremely low, of the order of  $0.5 \text{ W m}^{-1} \text{ K}^{-1}$  at 300 K regardless of the Sn content. Intriguingly, these values are the lowest reported to date among the different members of this family of compounds.<sup>[1,2]</sup> In the perpendicular direction, the values are higher, ranging between  $0.70$  and  $1.15 \text{ W m}^{-1} \text{ K}^{-1}$  at 300 K. The former are lower than those of the Bi-based counterparts but comparable to those measured in other chalcogenide systems such as SnSe or SnS, suggesting a significant degree of anharmonicity in the chemical bonding of  $\beta$ - $\text{As}_2\text{Te}_3$ .<sup>[1,2,37–41]</sup> The comparable magnitude in  $\kappa$  between these compounds is consistent with their similar acoustic phonon dispersions derived from ab initio calculations.<sup>[23,37,40]</sup>

The temperature dependence of the dimensionless figure of merit  $ZT$  calculated from the combination of the electrical and thermal transport properties is shown in Figure 3b. The  $ZT$  values increase, in the parallel direction, from  $0.56$  in undoped  $\beta$ - $\text{As}_2\text{Te}_3$  to  $0.65$  at  $423 \text{ K}$  in the  $x = 0.015$  sample. The  $ZT$  values appear nearly isotropic for all samples due to the compensation between the anisotropy in  $\rho(T)$  and  $\kappa(T)$ , both of which being opposite and of almost equal magnitude. Interestingly, these values are similar to those measured in undoped  $\text{Bi}_2\text{Te}_3$  leaving room for further optimization via alloying with, e.g.,  $\text{Bi}_2\text{Te}_3$  or  $\text{Bi}_2\text{Se}_3$ .<sup>[1,2]</sup> Because several other extrinsic dopants were shown to influence the transport properties in the Bi analogues, the present results also prompt further investigations to determine the nature and the concentration of the most beneficial doping element.

In summary, we demonstrated the successful synthesis of  $\beta$ - $\text{As}_2\text{Te}_3$ , another member of the well-known family of  $\text{Bi}_2\text{Te}_3$ -based thermoelectric alloys. We further showed that the transport properties can be tuned by extrinsic dopants, Sn providing herein a proof-of-principle. The similarities shared by  $\beta$ - $\text{As}_2\text{Te}_3$  with the Bi counterparts suggest that  $n$ -type electrical conduction might be equally achieved. Provided high-quality single-crystals become available, the present results might also have ramifications to the study of the proposed topological state of this compound. The possibility to control the electronic band structure through substitutions might help to achieve bulk band gap with inverted symmetry thereby allowing for a detailed study of the topological state at ambient pressure, as observed in the  $\text{Bi}_{1-x}\text{Sb}_x$  and  $\text{Pb}_{1-x}\text{Sn}_x\text{Se}$  systems.<sup>[42–44]</sup> In addition, preliminary measurements at low temperatures (Figure S6, Supporting Information) show that semiconducting behavior, with high bulk electrical resistivity of the order of  $4.5 \text{ } \Omega \text{ cm}$  at  $5 \text{ K}$ , is achieved in the  $x = 0.05$  specimen. This key property raises interesting possibilities as for the observation of signatures of topological surface-state transport in single-crystalline samples.<sup>[45]</sup>

## Experimental Section

Polycrystalline  $\text{As}_{2-x}\text{Sn}_x\text{Te}_3$  samples ( $x = 0.0, 0.010, 0.015, 0.025, 0.035, 0.050,$  and  $0.075$ ) were prepared by direct reaction of stoichiometric amounts of pure elements (As (Goodfellow, 99.99%, shots), Te (5N+, 99.999%, shots), and Sn (Strem Chemicals, 99.999%, shots)) sealed

under secondary vacuum in quartz tubes. The tubes were heated slowly up to 923 K at a rate of 10 K min<sup>-1</sup>, dwelt at this temperature for 2 h and finally quenched in room-temperature water. The resulting ingots were crushed into micron-sized powders and cold-pressed into cylindrical pellets of 10 mm in diameter under a pressure of 750 MPa. Remarkably, all the obtained ingots showed an experimental density higher than 95% of the theoretical density owing to the peculiar mechanical properties of the (Bi,Sb)<sub>2</sub>X<sub>3</sub> compounds, which originate from the atomic layers of the crystal structure only weakly bonded by van der Waals forces.<sup>[1],2]</sup>

The crystal structure was determined by powder X-ray diffraction (PXRD) at 300 K with CuK $\alpha$ <sub>1</sub> radiation using a Bruker D8 Advance instrument. The chemical homogeneity of the samples was checked by scanning electron microscopy (SEM) and energy dispersive x-ray (EDX) mapping using a Quanta FEG (FEI).

The thermoelectric properties were measured between 300 and 473 K on well-shaped samples cut with a diamond wire-saw (typical dimensions of 2 × 2 × 8 mm<sup>3</sup>). Owing to the anisotropic crystal structure of the present compounds, the transport properties were measured on samples cut both parallel and perpendicular to the pressing direction.  $\alpha$  and  $\rho$  data were collected using a ZEM-3 apparatus (ULVAC-RIKO). Thermal diffusivity  $a$  was measured by a laser flash technique (Netzsch LFA 427). The specific heat  $C_p$  was measured by differential scanning calorimetry (DSC Netzsch Pegasus). The thermal conductivity was then calculated via  $\kappa = aC_p d$ , where  $d$  is the density measured using the mass and the geometric dimensions of the densified pellets. The density was considered temperature-independent in the present case. The uncertainties for the measured properties are estimated to be about 3%, 7%, and 10% for  $\rho$ ,  $\alpha$ , and  $\kappa$ , respectively. The Hall coefficient  $R_H$  was measured at 300 K on parallelepiped-shaped samples using the AC transport option of a physical property measurement system (PPMS, Quantum Design) by sweeping the magnetic field between -1 and +1 T. The hole concentration  $p$  and Hall mobility  $\mu_H$  were estimated from  $p = 1/eR_H$  and  $\mu_H = R_H/\rho$ .

## Supporting Information

Supporting Information is available from the Wiley Online Library or from the author.

## Acknowledgements

The authors acknowledge the financial support from the French National Agency (ANR) in the frame of its program "PROGELEC" (Verre Thermo-Générateur "VTG").

Received: November 6, 2014

Revised: December 5, 2014

Published online:

- [1] CRC Handbook of Thermoelectrics (Ed: D. M. Rowe), CRC Press, New York 1995.
- [2] Thermoelectrics and Its Energy Harvesting (Ed: D. M. Rowe), CRC Press, New York 2012.
- [3] H. J. Goldsmid, Thermoelectric Refrigeration, Temple Press Books, Ltd., London 1964.
- [4] G. J. Snyder, E. S. Toberer, *Nat. Mater.* **2008**, *7*, 105.
- [5] L. Fu, C. L. Kane, *Phys. Rev. B* **2007**, *76*, 045302.
- [6] L. Fu, C. L. Kane, E. J. Mele, *Phys. Rev. Lett.* **2007**, *98*, 106803.
- [7] J. E. Moore, L. Balents, *Phys. Rev. B* **2007**, *75*, 121306.
- [8] M. Z. Hasan, C. L. Kane, *Rev. Mod. Phys.* **2010**, *82*, 3045.
- [9] X.-L. Qi, S.-C. Zhang, *Rev. Mod. Phys.* **2011**, *83*, 1057.
- [10] D. Hsieh, Y. Xia, D. Qian, L. Wray, F. Meier, J. H. Dil, J. Osterwalder, L. Patthey, A. V. Fedorov, H. Lin, A. Bansil, D. Grauer, Y. S. Hor, R. J. Cava, M. Z. Hasan, *Phys. Rev. Lett.* **2009**, *103*, 146401.
- [11] Y. Xia, D. Qian, D. Hsieh, L. Wray, A. Pal, H. Lin, A. Bansil, D. Grauer, Y. S. Hor, R. J. Cava, M. Z. Hasan, *Nat. Phys.* **2009**, *5*, 398.
- [12] Y. L. Chen, J. G. Analytis, J.-H. Chu, Z. K. Liu, S.-K. Mo, X. L. Qi, H. J. Zhang, D. H. Lu, X. Dai, Z. Fang, S. C. Zhang, I. R. Fisher, Z. Hussain, Z.-X. Shen, *Science* **2009**, *325*, 178.
- [13] P. Roushan, J. Seo, C. V. Parker, Y. S. Hor, D. Hsieh, D. Qian, A. Richardella, M. Z. Hasan, R. J. Cava, A. Yazdani, *Nature* **2009**, *460*, 1106.
- [14] D.-X. Qu, Y. S. Hor, J. Xiong, R. J. Cava, N. P. Ong, *Science* **2010**, *329*, 821.
- [15] N. P. Butch, K. Kirshenbaum, P. Syers, A. B. Sushkov, G. S. Jenkins, H. D. Drew, J. Paglione, *Phys. Rev. B* **2010**, *81*, 241301.
- [16] Z. Ren, A. A. Taskin, S. Sasaki, K. Segawa, Y. Ando, *Phys. Rev. B* **2010**, *82*, 241306.
- [17] M. Saghier, M. R. Lees, S. J. York, G. Balakrishnan, *Cryst. Growth Des.* **2014**, *14*, 2009.
- [18] M. Safdar, Q. Wang, M. Mirza, Z. Wang, J. He, *Cryst. Growth Des.* **2014**, *14*, 2502.
- [19] M. Safdar, Q. Wang, M. Mirza, Z. Wang, K. Xu, J. He, *Nano Lett.* **2013**, *13*, 5344.
- [20] Z. Li, S. Shao, N. Li, K. McCall, J. Wang, S. X. Zhang, *Nano Lett.* **2013**, *13*, 5443.
- [21] T. Scheidemantel, J. Meng, J. Badding, *J. Phys. Chem Solids* **2005**, *66*, 1744.
- [22] H. W. Shu, S. Jaulmes, J. Flahaut, *J. Solid State Chem.* **1988**, *74*, 277.
- [23] K. Pal, U. V. Waghmare, *Appl. Phys. Lett.* **2014**, *105*, 062105.
- [24] Y. Sharma, P. Srivastava, *Opt. Mater.* **2011**, *33*, 899.
- [25] A. Chelkowski, E. Talik, G. Wnetrzak, *Mater. Res. Bull.* **1986**, *21*, 1509.
- [26] L. P. Caywood Jr., G. R. Miller, *Phys. Rev. B* **1970**, *2*, 3209.
- [27] A. Vasko, L. Tichy, J. Horak, J. Weissenstein, *Appl. Phys.* **1974**, *5*, 217.
- [28] Y. S. Hor, A. J. Williams, J. G. Checkelsky, P. Roushan, J. Seo, Q. Xu, H. W. Zandbergen, A. Yazdani, N. P. Ong, R. J. Cava, *Phys. Rev. Lett.* **2010**, *104*, 057001.
- [29] C. M. Jaworski, J. Tobola, E. M. Levin, K. Schmidt-Rohr, J. P. Heremans, *Phys. Rev. B* **2009**, *80*, 125208.
- [30] A. J. Strauss, *J. Electron. Mater.* **1973**, *2*, 553.
- [31] H. Süßmann, K. Loof, *Phys. Status Solidi* **1973**, *37*, 467.
- [32] J. Horak, K. Cermak, L. Koudelka, *J. Phys. Chem. Solids* **1986**, *47*, 805.
- [33] J. Navratil, P. Lostak, J. Horak, *Cryst. Res. Technol.* **1991**, *26*, 675.
- [34] P. Lostak, J. Navratil, J. Sramkova, J. Horak, *Phys. Status Solidi A* **1993**, *135*, 519.
- [35] S. Santhanam, N. J. Takas, W. M. Nolting, P. F. P. Poudeu, K. L. Stokes, *Mater. Res. Soc. Sym. Proc.* **2011**, *1329*, 101.
- [36] V. A. Kulbachinskii, V. G. Kytin, A. A. Kudryashov, R. A. Lunin, *J. Solid State Chem.* **2012**, *193*, 83.
- [37] L.-D. Zhao, S.-H. Lo, Y. Zhang, H. Sun, G. Tan, C. Uher, C. Wolverton, V. P. Dravid, M. G. Kanatzidis, *Nature* **2014**, *508*, 373.
- [38] S. Sassi, C. Candolfi, J.-B. Vaney, V. Ohorodniichuk, P. Masschelein, A. Dauscher, B. Lenoir, *Appl. Phys. Lett.* **2014**, *104*, 212105.
- [39] C.-L. Chen, H. Wang, Y.-Y. Chen, T. Day, J. Snyder, *J. Mater. Chem. A* **2014**, *2*, 11171.
- [40] J. Carrete, N. Mingo, S. Curtarolo, *Appl. Phys. Lett.* **2014**, *105*, 101907.
- [41] Q. Tan, L.-D. Zhao, J.-F. Li, C.-H. Wu, T.-R. Wei, Z.-B. Xing, M. G. Kanatzidis, *J. Mater. Chem. A* **2014**, *2*, 17302.
- [42] D. Hsieh, D. Qian, L. Wray, Y. Xia, Y. S. Hor, R. J. Cava, M. Z. Hasan, *Nature* **2008**, *452*, 970.
- [43] F. Nakamura, Y. Kousa, A. A. Taskin, Y. Takeichi, A. Nishide, A. Kakizaki, M. D'Angelo, P. Lefevre, F. Bertran, A. Taleb-Ibrahimi, F. Komori, S.-I. Kimura, H. Kondo, Y. Ando, I. Matsuda, *Phys. Rev. B* **2011**, *84*, 235308.
- [44] P. Dziuba, B. J. Kowalski, K. Dybko, R. Buczko, A. Szczerbabow, M. Szot, E. Lusakowska, T. Balasubramanian, B. M. Wojek, M. H. Berntsen, O. Tjernberg, T. Story, *Nat. Mater.* **2012**, *11*, 1023.
- [45] J. Xiong, A. C. Petersen, D. Qu, Y. S. Hor, R. J. Cava, N. P. Ong, *Physica E* **2012**, *44*, 917.